01 Jan 1997

A System for Collecting Milligram Quantities of Cloud Condensation Nuclei

Darryl J. Alofs
Missouri University of Science and Technology, dalofs@mst.edu

Donald E. Hagen
Missouri University of Science and Technology, hagen@mst.edu

Steven D. Medley

Daniel R. White
Missouri University of Science and Technology

et. al. For a complete list of authors, see https://scholarsmine.mst.edu/mec_aereng_facwork/5023

Recommended Citation

D. J. Alofs et al., "A System for Collecting Milligram Quantities of Cloud Condensation Nuclei," *Aerosol Science and Technology*, vol. 26, no. 5, pp. 415 - 432, Taylor and Francis Group; Taylor and Francis, Jan 1997.
The definitive version is available at https://doi.org/10.1080/02786829708965442

Aerosol Science and Technology

ISSN: 0278-6826 (Print) 1521-7388 (Online) Journal homepage: https://www.tandfonline.com/loi/uast20

A System for Collecting Milligram Quantities of Cloud Condensation Nuclei

Darryl J. Alofs , Allen L. Williams , Donald E. Hagen , Steven D. Medley , Daniel R. White & John Schmitt

To cite this article: Darryl J. Alofs , Allen L. Williams , Donald E. Hagen , Steven D. Medley , Daniel R. White & John Schmitt (1997) A System for Collecting Milligram Quantities of Cloud Condensation Nuclei, Aerosol Science and Technology, 26:5, 415-432, DOI: 10.1080/02786829708965442

To link to this article: https://doi.org/10.1080/02786829708965442

Published online: 13 Jun 2007.

A System for Collecting Milligram Quantities of Cloud Condensation Nuclei

Darryl J. Alofs, Allen L. Williams, Donald E. Hagen, Steven D. Medley, Daniel R. White, and John Schmitt*

CLOUD AND AEROSOL SCIENCE LABORATORY, 1870 MINER CIRCLE, UNIVERSITY OF MISSOURI—ROLLA, ROLLA, MO 65409 (D.J.A.; D.E.H.; S.D.M.; J.S.), AND ATMOSPHERIC SCIENCES DIVISION, ILLINOIS STATE WATER SURVEY, 2204 GRIFFITH DRIVE, CHAMPAIGN, IL 61820 (A.L.W.)

ABSTRACT. An experimental system to collect cloud condensation nuclei (CCN) onto filters in amounts sufficient for chemical analysis is described. This experimental apparatus is designed to process ambient air at a rate of more than 1 m^3/min. Two identical systems have been built. One is installed in a laboratory at Rolla, MO. The other is installed on an 11 m long trailer. The system isolates three size classes of CCN, having mass median diameters of 0.27, 0.12, and 0.075 μm, respectively, and mass collection rates of 11.5, 1.28, and 0.13 mg/day, respectively. The above sizes and collection rates are obtained from a computer simulation that does not account for particle evaporation, but tests of the system indicate that there is particle evaporation which produces some change in the sizes and collection rates. The system components were tested by sampling laboratory-generated CCN of different selected sizes, and the test results were used as inputs for the computer simulation of the system performance. AEROSOL SCIENCE AND TECHNOLOGY 26:415–432 (1997)

INTRODUCTION

Cloud condensation nuclei (CCN) constitute a small mass fraction of the ambient aerosol. They form droplets at a supersaturation of 1%, which corresponds to a relative humidity of 101%. The size of the more numerous CCN is less than 0.1 μm diameter, while most of the CCN mass is in larger particles. Collecting CCN in sufficient amounts to determine their chemical composition is complicated by low ambient CCN mass concentrations and the probability of a few large CCN dominating the sample mass.

The purpose of determining CCN compositions is to identify and quantify their sources. Although this is an important fundamental issue from the standpoint of cloud physics, the subject has gained additional significance in relation to the "direct" (Charlson et al., 1992; Kiehl and Briegleb, 1993) and "indirect" (Twomey et al., 1984; Charlson et al., 1987; Wigley, 1989) aerosol effects associated with global warming. The direct effect on the atmospheric heat balance is caused by the scattering of sunlight by anthropogenic aerosols and haze particles, and is mainly due to particles from 0.2 to 0.5 μm diameter (Ensor et al., 1972; Schwartz, 1996). The indirect effect is

* Corresponding author.

Aerosol Science and Technology 26:415–432 (1997)

Published by Elsevier Science Inc.

0278-6826/97/$17.00
PII S0278-6826(97)00041-X

caused by higher anthropogenic CCN concentrations, giving rise to more numerous, smaller cloud drops, which results in more sunlight being reflected back to space. Both effects appear to result in cooling, and are thought to compensate in part for the warming from increasing carbon dioxide.

It is widely thought that CCN and haze compositions are dominated by ammonium sulfate, based largely on experiments by Twomey (1971), which show that CCN volatilize at nearly the same temperature as ammonium sulfate. In industrialized regions, anthropogenic sulfur dioxide emissions dominate natural sulfur sources, and the resulting sulfate aerosol formation is a plausible dominant continental CCN source. Diesel exhaust is a known strong anthropogenic CCN source (Hudson, 1991), and the CCN concentrations downwind of major cities are high. Biomass burning is a strong CCN source (Warner and Twomey, 1967; Hudson et al., 1991) that can be either natural or anthropogenic, although in modern times, such emissions are estimated to be predominantly anthropogenic (Hileman, 1990).

Natural continental CCN sources are, apparently, widely dispersed and not well documented; the large anthropogenic continental sources obscure the study of natural continental sources. Curiously, despite the high anthropogenic sulfur dioxide emissions over North America, the CCN concentrations over less industrialized regions of Australia and Africa are comparable to those over the eastern United States (Twomey and Wojciechowski, 1967). Dimethylsulfide emissions from the ocean, followed by atmospheric processes that result in sulfate aerosol formation, represent a plausible major natural source of maritime CCN (Charlson et al., 1987; Fitzgerald, 1991). Continental CCN concentrations are uniformly much higher than maritime levels; however, the extent to which this is due to anthropogenic sources, implying substantial alteration of natural conditions, is an unsettled issue.

These questions suggest the need for identifying the sources of CCN, and a plausible strategy for doing this is to determine their chemical composition. A large sample would enable measurement of not only the major constituents, but also species found in smaller quantities that may be important as chemical tracers of the sources. Harrison (1985) developed a technique for collecting CCN in large quantities by forming droplets in a large continuous flow diffusion cloud chamber (CFD), and removing the droplets by a virtual impactor downstream of the CFD. Since aerosol particles as large as 1 μm were drawn into the system, the CCN composition from this device would likely be dominated by the composition of the larger CCN particles. Novakov and Penner (1993) collected aerosol on the stages of a micro-orifice impactor (Marple et al., 1991), and determined the relative amounts of organics, ammonium sulfate, and sodium chloride. The drawbacks of this technique are the lack of a positive identification of CCN as those particles that activate droplets and the necessarily small amount of mass obtained on the impactor stages due to the limited flow rate.

A MODEL FOR HYGROSCOPIC BEHAVIOR OF ATMOSPHERIC CCN

The design of the collection system requires a model for the hygroscopic behavior of atmospheric particles, a model which predicts, for each dry size, the equilibrium size at 100% relative humidity and the critical supersaturation. Tandem differential mobility analyzer (TDMA) measurements indicate that for the size range 0.05–0.3 μm, atmospheric particles consist of two populations, one of which is more hygroscopic than the other (Zhang et al., 1993; Pitchford and McMurry, 1994; Svenningsson et al., 1994). Particles in the less hygroscopic group grow only slightly as humidity increases. For the sake of simplicity, we will assume that particles in the less hygroscopic population are completely nonhygroscopic and perfectly wettable, so that the size versus critical supersaturation is given by the Kelvin equation (Pruppacher and Klett, 1978, p.139). The model adopted for

the more hygroscopic particles is based on the measurements of Alofs et al. (1989) and of Fitzgerald et al. (1982).

A one-year sampling program (Alofs et al., 1989) showed that atmospheric particles with dry diameter of 0.2, 0.3, and 0.4 μm grew to an equilibrium size at 100% relative humidity as if they were composed of 50% by volume ammonium sulfate and 50% insoluble material. Fitzgerald et al. (1982) performed measurements on atmospheric particles in the dry size range 0.04–0.1 μm to determine the relation between dry size and critical supersaturation. When cast in terms of an apparent volume fraction of ammonium sulfate, their measurements also indicate 50% ammonium sulfate (Alofs et al., 1989). The hygroscopic particles in the two-population model are assumed to be 50% ammonium sulfate by volume and 50% insoluble material. Inertial separation is used in the collection system, so the density of the atmospheric particles must be assumed to predict performance. The assumed specific gravity of hygroscopic particles is 1.384 and of insoluble particles is 1.000. Adoption of these model compositions should not be construed as belief that these are the actual atmospheric compositions, but rather that these are compositions which give the actual mean hygroscopic behavior of the two populations of atmospheric particles. The relative numbers of these two populations are discussed next.

DECISION OF WHAT SIZE CCN TO COLLECT

Knowledge of the size distribution of CCN and of the total population of atmospheric particulates is of help in forming a strategy for collecting CCN samples for chemical analysis. During the period November 1–20, 1994, the atmospheric aerosol at the University of Missouri—Rolla site (Alofs et al., 1989) was sampled almost continuously. A mixture of filtered dry air and atmospheric air was passed through a differential mobility analyzer (DMA) (Liu and Pui, 1974) under conditions such that the particles were close to their dry size while passing through the DMA. The monodispersed flow out of the DMA was monitored for total particle concentration, and for concentration of particles active at 1% supersaturation, using a TSI 3025A counter (TSI Incorporated, St. Paul, MN) and a CFD (Alofs, 1978), respectively. The voltage of the DMA was swept in steps to obtain electrical mobility distributions, and these distributions were inverted using the method of Hagen and Alofs (1983) to obtain size distributions. The averages from 126 voltage sweeps are shown as two differential size distributions in Fig. 1. One curve (labeled CNC) is for all particles; the other is for the CCN. Note that the two curves merge at 0.125 μm, indicating that all particles larger than this size are CCN. For increasingly smaller sizes, nonhygroscopic particles become relatively more numerous. At about 0.028 μm diameter, the CFD count is nearly zero. Figure 2 shows the same data, converted to volume distributions. The differences in the two volume distributions for large particles are ascribed to instrumentation errors.

Figures 1 and 2 and related earlier measurements (Alofs and Trueblood, 1983) influenced the decision concerning what size CCN to collect. The peak in the number distribution of the CCN is at 0.068 μm diameter. Since the indirect effect of CCN on climate depends more on number of CCN rather than size, one might argue for collecting a mass median diameter near 0.068 μm. This would require rejecting particles which are not CCN because the two curves of Fig. 1 are distinct at this size. Also, from Fig. 2, it can be seen that if the sample has a mass median diameter of 0.068 μm, the mass will be small in comparison with that collected if one copies the Harrison (1985) choice to collect all CCN smaller than 1 μm diameter. Either micro-orifice (Marple et al., 1991) or low-pressure impactors (Hering et al., 1978) have sufficiently small cut-points to achieve the required exclusion of the larger particles for a 0.068 μm mass median diameter sample. The flow of these impactors, however, is low (30 and 1.0 L/min, respectively), and

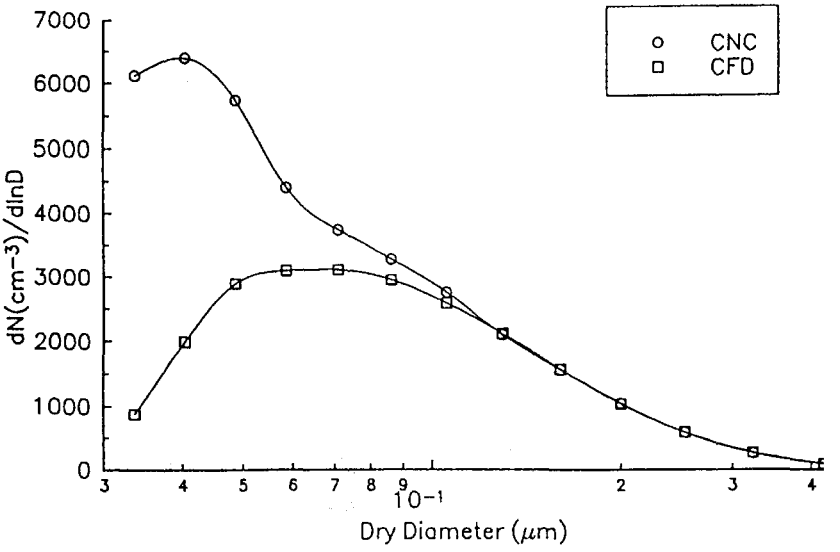

FIGURE 1. Measured size distribution of atmospheric particles as detected by a condensation nucleus counter (CNC) and a continuous flow diffusion (CFD) cloud chamber with an operating supersaturation of 1%.

for the latter case, there is concern that semi-volatile organics will evaporate at the low pressure (56 mm Hg.) For the micro-orifice impactor, which is normally operated as a cascade impactor, there is concern that the micro-orifices would quickly plug up if the upstream stages were removed and atmospheric air passed directly into the final stage.

In view of the above difficulties in collecting only the small, more numerous CCN, and in view of the argument about to be

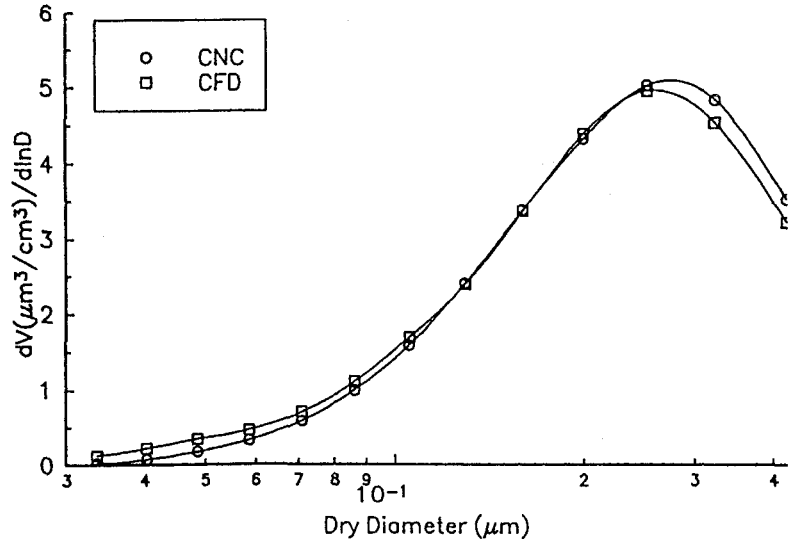

FIGURE 2. Volume distributions computed from the Fig. 1 number distributions.

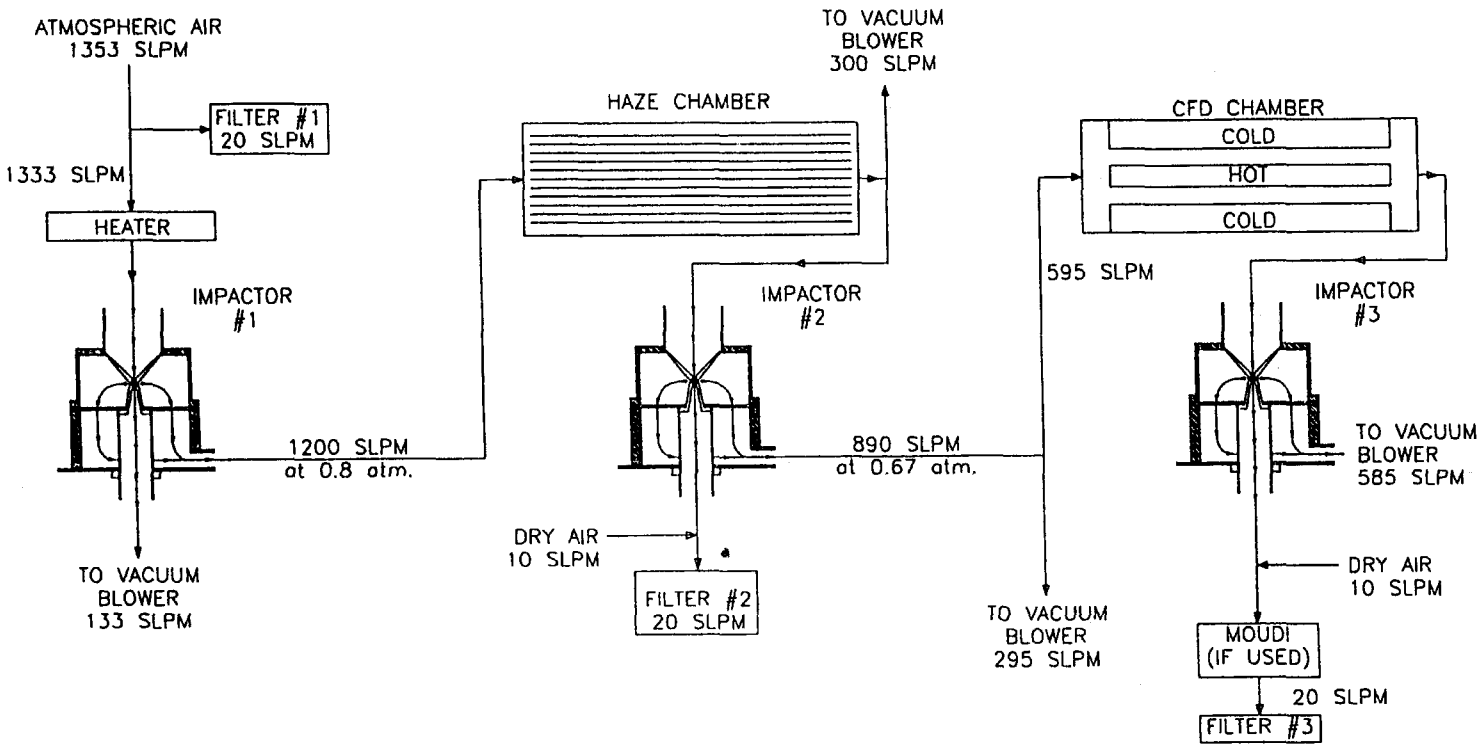

FIGURE 3. Overall schematic of the collection system. SLPM means standard liters per minute.

given, it seems prudent to collect CCN in a variety of size ranges. The Novakov and Penner (1993) results indicate the importance of organic compounds for CCN, but do not identify particular organic compounds. Techniques for identifying specific organic compounds require knowing what species one is looking for. It was anticipated that the advantage of high sample mass would allow identification of specific organic compounds for larger CCN. Once specific organics were identified in large CCN, one then could look for these compounds more efficiently in samples of small CCN. Also, knowledge of the chemical composition versus size would perhaps be of use in surmising the history of CCN formation and growth.

Once the decision is made to collect CCN in a variety of separate size ranges, the question remains as to how to do it. One possibility for alleviating the difficulty of achieving small impactor cut-size is to humidify the air so as to enlarge the particle diameter by a factor which turns out to be about a factor of 4. As shown below, a virtual impactor with a cut-point of 0.5 μm diameter can be built with modest pressure drop, and with large enough orifice dimension (0.0254 cm) to avoid plugging. For the model atmospheric hygroscopic particles, a 0.12 μm dry size produces a 0.5 μm diameter haze drop at 100% relative humidity. This factor of 4 reduction in cut-point is a great advantage for reduction of impactor pressure drop and reduction of the tendency of the impactor orifices to plug up.

SIMPLE ANALYSIS OF SYSTEM

Figure 3 is a schematic of the collection system chosen. The heater at the system inlet assures that the particles will be dry as they pass through impactor 1, which has a cut-point of 0.5 μm and is a virtual impactor. Thus, particles above the cut-point size pass into the minor flow outlet stream, and particles below the cut-point pass into the major flow outlet stream, which flows into the haze chamber. The haze chamber is an adiabatic humidifier, whose temperature is controlled by the heater upstream of impactor 1. In the haze chamber, the hygroscopic particles grow to form haze drops at 100% relative humidity. These haze drops pass directly into impactor 2, which has a haze drop cut-point of 0.5 μm, equivalent to a dry cut-point of 0.12 μm for the model atmospheric hygroscopic particles. Hygroscopic particles in the minor flow of impactor 2 thus are in the size range 0.12–0.5 μm dry diameter. This size range is based on the simplifying assumption of very high size resolution for the impactors. The minor flow of impactor 2 is mixed with dry air, and then passes through filter 2 where the particles are collected.

The major flow of impactor 2, containing nonhygroscopic particles smaller than 0.5 μm diameter and hygroscopic particles smaller than 0.12 μm, passes through a long pipe and then into the CFD cloud chamber, which operates at 0.6% supersaturation. According to the Kelvin equation, nonhygroscopic particles having critical supersaturation below 1% and 0.6% have diameters above 0.23 and 0.4 μm, respectively. If the CFD operates at a supersaturation of 1.0%, nonhygroscopic particles in the size range 0.23–0.5 μm would be activated. If it operates at 0.6% supersaturation, the undesirable nonhygroscopic particles are in the smaller range of 0.4–0.5 μm diameter. Fortunately, Fig. 1 indicates that in any case, there should be very few such undesirable nonhygroscopic particles. Initially, it was planned that the CFD would be operated at 1% supersaturation, but after the system was built, the standard operation was moved to 0.6% supersaturation. This decision was made just in case, at some geographic locations, there are more insoluble particles than Fig. 1 indicates. When the CFD supersaturation was reduced, the CFD residence time had to be increased in order to maintain the 1.5 μm drop size at the CFD exit. This was achieved by throwing away about half the flow out of the haze chamber, as shown in Fig. 3.

Particles which activate in the CFD and grow to droplets larger than the 1.0 μm diameter cut-point of impactor 3 are col-

lected on filter 3. The size of model atmospheric hygroscopic particles with a critical supersaturation of 0.6% is 0.05 μm diameter. Thus, hygroscopic particles on filter 3 have sizes in the diameter range 0.050–0.12 μm. As an alternative to filter 3, the minor flow of impactor 3 can be passed through stage 8 of a commercial micro-orifice uniform deposit impactor (MOUDI) (Marple et al., 1991). In this case, let filter 3 be called filter 3M, which then collects CCN having a mass median diameter of 0.075 μm.

The above analysis is somewhat simplistic, but a more detailed analysis and performance measurements given below show that, in most respects, the simple analysis is not misleading. Before leaving the simple analysis, consider possible alterations of the chosen collection system. One could eliminate the haze chamber and impactor 2, and decrease the cut-point of impactor 1 to 0.12 μm. The collection at filters 3 and 3M would be approximately unaffected, and there would be no filter 2. The loss of filter 2 would turn out to be a severe loss because it turns out that the chemical composition is quite different at filters 2 and 3. These chemical composition data will be presented in a later paper, but suffice it to say here that there is considerably less organic material at filter 2 than at filter 3. Also, removal of the haze chamber would increase greatly the weight of the CFD because the relative humidity coming into the CFD would be less, which would require a more positive means of controlling hot plate temperature than in the present design. Also, reducing the cut-point of impactor 1 from 0.5 to 0.12 μm is far from trivial. One possibility would be to decrease the orifice size from 0.0254 to 0.00308 cm, while keeping the jet velocity constant at 172 m/s. Aside from the mechanical difficulties of accuracy in machining, the orifice is likely to be quickly plugged. The plugging problem could be helped by putting coarse impactor stages upstream of impactor 1, but this increases complexity and pressure drop. Another alternative would be to go above 172 m/s impactor nozzle jet velocity, but the Mach number is already 0.51 and cannot be increased above unity without introducing undesirable normal shock waves.

HAZE CHAMBER AND HEATER

The physical details of the haze chamber are as follows. It consists of a box containing vertical aluminum plates spaced 1 cm apart, and covered with cotton cloth which is kept wet with deionized water supplied at the top edge of each plate. Excess water which has run down the plates is recirculated after passing through a water cleanup system. There are nine inner plates which are wet on both sides, and two outer plates which are wet on one side and are thermally insulated on the other side. The two outer plates are part of the box that forms the enclosure. The plates are each 3.6 m long in the horizontal direction and 1.2 m high in the vertical direction. The sample flows horizontally in the 1 cm space between the plates. The mean velocity is 18 cm/s and the Reynolds number is 153. The air reaches 100% relative humidity as it passes through the haze chamber. The total mean resident time of 20 s is sufficient for hygroscopic particles to grow to their equilibrium size or to 0.5 μm diameter, whichever is smaller. Between the outlet of impactor 1 (see Fig. 3) and the inlet to the haze chamber, there is a manifold system to distribute the inlet flow in the 1.2 m vertical direction.

At the outlet end of the haze chamber, the air converges through an exit slot 2.54 cm wide in the horizontal direction by 31 cm long in the vertical direction. Impactor 2 mounts directly on this exit slot. Air at the top and bottom of the slot is thrown away, and just the core flow passes into the impactor (see Fig. 3). This was done for two reasons. First, the plates do not reach completely to the top of the haze chamber enclosure, and hence air flowing along the top reaches 100% relative humidity too late to let the suspended haze drops reach the equilibrium sizes. Second, the vortices formed as the flow bends around the top

and bottom corners of the slot are thereby removed and prevented from entering impactor 2. Tests showed that these changes from the original design improved the performance of the haze chamber–impactor 2 system.

The haze chamber has the simplicity of being an adiabatic device, thus avoiding the complication of *in situ* active thermal control of the 80 m^2 meters of wet surface presented by the plates. The temperature control is achieved by preheating the air before it passes into the haze chamber. The control parameter for the heater (Fig. 3) is the wet bulb temperature at the heater exit. The heater is turned on and off by a commercial controller to compensate for time variations of atmospheric temperature and relative humidity, such that the air coming into the haze chamber has a time-invariant wet bulb temperature, even though the dry bulb temperature will vary as atmospheric conditions vary. The heater is a shell and tube heat exchanger, with the sample air flowing through the tubes and with heated water flowing through the shell. The time response of the heater is about 10 min, which is sufficiently fast to compensate for diurnal variations of atmospheric conditions.

The plate temperature of the haze chamber adjusts to the wet bulb temperature of the incoming air by convective heat and water vapor exchange with the air, similar in principle to the operation of a wet bulb thermometer. At any location on the plates, the surface is receiving sensible heat from the warmer air, but is losing an equal amount of latent heat due to evaporation. Experiments by Carrier and Lindsay (1924) and calculations by Sparrow and Chen (1969) show that the resulting plate temperature is very nearly isothermal at the wet bulb temperature of the incoming air.

The preheater is always set so that the temperature of the air is raised by at least 6°C in order that the particles will be near their dry size as they pass through impactor 1 (Fig. 3). This means that the relative humidity at impactor 1 will be below 70%. According to the measurements of Hänel (1976), this assures that atmospheric particles in the size range of interest will have a diameter not larger than 12% above the dry diameter. The hygroscopic behavior of atmospheric particles shows a hysteresis effect, and since humidity falls as the air passes through the heater, the Hänel data for falling relative humidity are applicable.

As an example of preheater temperatures, if the heater is set to a wet bulb temperature of 27.9°C, and the daytime ambient temperature and relative humidity are 21°C and 80%, respectively, the temperature exiting the heater is 55.6°C. If, say, during the subsequent evening, atmosphere temperature and relative humidity change to 13°C and 70%, the temperature exiting the heater is 69.4°C. Downstream of the heater, the sample then passes through impactor 1, and because of the pressure drop across this impactor, the wet bulb temperature drops to 25°C. Thus, the haze chamber would operate at 25°C during both the daytime and nighttime conditions of this example. As the seasons change, the wet bulb temperature setting must be changed. During a Missouri winter, it would be lowered to 15°C to avoid excessive temperatures coming out of the heater. In the summer, it would be raised to 40°C to assure that the particles are dry at impactor 1.

CFD CLOUD CHAMBER

The CFD cloud chamber (Fig. 3) consists of three vertical plates, each 1.2 m high by 3.6 m long. Like the haze chamber plates, these plates are wet and are spaced 1 cm apart, with the air flowing horizontally in the 1 cm space between them. The mean velocity is 64 cm/s, the mean residence time is 5.7 s, and the Reynolds number is 650. The inner plate, or hot plate, is heated to 22°C by internal heaters. The heaters provide vertically uniform and horizontally adjustable heat flux. The adjustments to achieve an isothermal hot plate are minor because the incoming air has a wet bulb temperature that matches the hot plate temperature. Since the wet bulb temperature drops be-

tween the haze chamber and the CFD inlet because of pressure drop across impactor 2, the hot plate temperature is set slightly below the haze chamber temperature. Both sides of the hot plate are covered with cotton cloth, and deionized water is supplied at the top edge in sufficient quantity to keep the surfaces of the plate uniformly wet. To cool the outer plates, or cold plates, water flows through jackets, and maintains their temperature at 18.2°C. The surfaces of the cold plates are kept wet by the condensation forming on them. If the haze chamber were left out of the system, the hot plate of the CFD would require a more active thermal control, such as a water jacket, to achieve an isothermal condition, and the weight of the CFD would be approximately doubled.

A parabolic supersaturation profile is produced between adjacent hot and cold plates with a peak value of 0.6% midway between the plates and 0% supersaturation (100% relative humidity) at the plate surfaces. Particles with critical supersaturation (S_c) at or below the supersaturation (S) value they encounter in the CFD are activated, and undergo diffusional growth to approximately 1.5 μm diameter during their residence in the CFD. The final drop size coming out of the CFD is approximately proportional to both local supersaturation and growth time. Since both the velocity profile and the supersaturation profile are parabolic, droplets near the wall experience longer growth time and lower supersaturation than those midway between the walls. Thus, the drop size is almost independent of position between the plates. However, the behavior of a population of particles passing through the CFD is sufficiently complicated that a computer model has been developed to interpret the expected response of particles in the entire system including the CFD.

IMPACTOR DESIGN

All three virtual impactors are of a rectangular design with slit length of 30.48 cm. They are constructed in four anodized aluminum sections that fit together with O-ring seals, as shown in the cross-sectional view in Fig. 4. The modular design allows for machining and assembly without seams in the plane of symmetry, except for the collection cup, which is a two-piece design with a lengthwise seam. Region I is the nozzle, which is a converging passageway which accelerates the flow. Region III is the collection cup, with its slit for collecting particles larger than the cut-point. Region IV is the base section, which contains passageways for both the minor flow and the major flow. Region II is the spacer section, which holds the nozzle and the collection

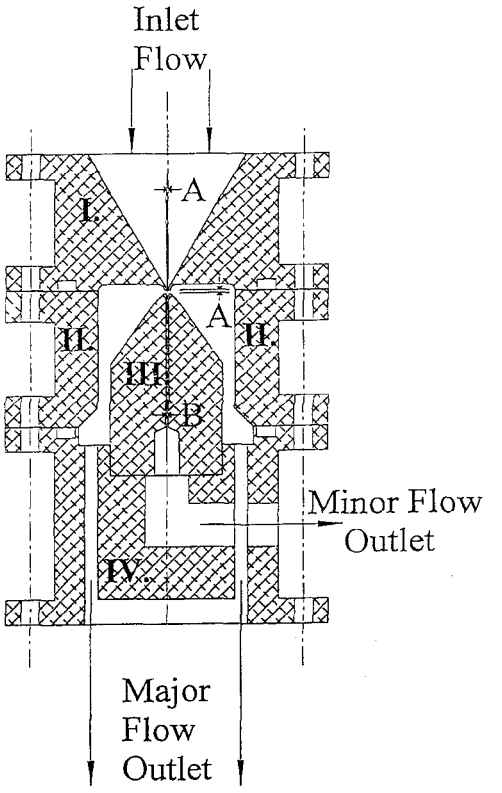

FIGURE 4. Cross-sectional view of impactors showing the nozzle inlet section (I), the spacer section (II), the collection cup (III), and the base (IV). Dimension (A) is 0.51 mm for impactor 2 and 0.89 mm for impactor 3, while dimension B is 0.76 mm for impactor 2 and 1.30 mm for impactor 3.

cup in precise alignment and which, together with regions III and IV, forms the passageway for the major flow.

Impactors 1 and 2, with 0.5 μm cutoffs, have the same critical dimensions: the inlet slit width and the spacing between the inlet slit and the cup (dimension A) are each 0.51 mm, and the collection cup slit width is 0.76 mm (dimension B). The corresponding dimensions for impactor 3 are 0.89 and 1.30 mm and the cutoff particle diameter is 1.0 μm. In order to ensure uniform minor flow across the entire slit length, the collection cup is internally partitioned into six equal sections through which the flow is drawn separately. The flow was simulated using a commercial fluid dynamics code (Fluid Dynamics International, Inc.) to aid in setting critical parameters. Alterations in the original design were made to reduce particle loss when, after prolonged sampling of latex spheres, visible deposits were noted. Both the regions below the inlet slit in the entrance section and the shoulder of the collection cup were streamlined in this way. Further guidance concerning the reduction of particle losses was also taken from the work of Chen and Yeh (1987).

TRANSIENT SUPERSATURATION IN IMPACTOR 2

Under the assumption of isentropic flow in the nozzle of impactor 2 (see region I of Fig. 4), a supersaturation of 112% is produced at the exit of the nozzle, where the air velocity is 172 m/s (Mach number equal to 0.51). Droplet growth calculations indicate that a haze drop 0.5 μm diameter at nozzle entrance will grow to 0.5022 μm diameter at nozzle exit. This growth is so small because of the short residence time (7.6 ms) in the nozzle, and means that inertial separation of particles near the cutoff size will not be influenced by the supersaturation developed in impactor 2.

A second conceivable effect of transient supersaturation would be to increase losses within the impactor. It could be that, after inertial separation of the particles, the transient supersaturation persists in the major-flow passageways. This might lead to drop sizes sufficiently large that there is some secondary impaction onto the walls. The transient supersaturation does not persist in the minor-flow passageways because the pressure recovery is quite complete so that the minor flow has the same pressure as at the impactor inlet. The losses were measured for the impactor (see Fig. 6), and are larger than Chen and Yeh (1987) report for their dry virtual impactor with a 2.5 μm cut-point. The losses are not so large as to greatly decrease sample loadings, and hence are not a serious shortcoming.

Consider this third possible effect of transient supersaturation. The peak in the Köhler curve (Pruppacher and Klett, 1978, p. 142) is at a size called the critical size, and nuclei which reach this size are said to have activated because the supersaturation required to keep then continuously growing decreases as they grow further. As S_c increases, the critical size decreases, and hence for a fixed supersaturation, the time to activate decreases. Thus, there are very small nuclei which activate due to the transient supersaturation. Growth calculations show that they do not reach 0.5 μm, so these activated nuclei will end up in the major flow. Is there any chance they would still be activated when they reach the CFD? This would be a problem because then they might continue to grow in the CFD, even though their S_c exceeds 0.6%. The answer is "no" because such nuclei would deactivate in the 5.24 cm diameter pipe between impactor 2 and the CFD. The relative humidity in the pipe is 82% over the entire 4.6 m length of the pipe, and particles are in the pipe for at least 0.333 s.

TESTS WITH ARTIFICIAL AEROSOLS

The apparatus was tested by measuring the efficiencies with which test aerosols were transmitted to various points in the system. The aerosols for testing impactor 1 were generated by atomizing suspensions of polystyrene latex particles. The aerosols for testing other components were generated by atomizing aqueous solutions of sodium

chloride or uranine. Downstream of the atomizer, the aerosol passed first through a diffusion drier, then through a differential mobility analyzer (DMA). The DMA selects only particles in a narrow range of electrical mobility (Liu and Pui, 1974), and (if the inlet size distribution has been judiciously chosen) provides a test aerosol of particles with a narrow range of diameter. A high efficiency particulate air (HEPA) filter was placed upstream of the heater (Fig. 3) to remove ambient aerosol particles, and the test aerosol was inserted at various points depending on the part of the system being tested. A low-pressure version of the small CFD described by Alofs (1978) was used to measure concentrations of the test aerosol at the insertion point and the major and minor flows of the impactors.

The ordinate of Fig. 5 shows the measured transmission efficiency from the inlet of an impactor to either the major or the minor flow. Consider the solid curve, which is for the major flow of impactor 1, which was obtained using polystyrene latex test aerosols. The horizontal axis is the equivalent dry diameter of an atmospheric particle having the same Stokes number as the latex particle. The atmospheric particle is assumed to have a specific gravity of 1.384. Consider next the dashed curve, which is for the minor flow of impactor 2. The horizontal axis for this curve is the dry size of a model atmospheric hygroscopic particle, and the conversion to this from the sodium chloride or uranine aerosol dry size is performed as follows: Köhler theory (Pruppacher and Klett, 1978, p. 142) is used to compute the critical supersaturation of the test aerosol from the size of the test aerosol, and then again to calculate the dry size of an atmospheric particle with the same critical supersaturation as the test aerosol. The basis for this size conversion is that, according to Köhler theory, the relation between S_c and D_e (where D_e is the equilibrium droplet diameter at 100% relative humidity) does not depend on the chemical composition of the partially soluble particle (Laktionov, 1972).

The product of the efficiencies from the two curves of Fig. 5 gives the transmission efficiency of atmospheric particles to filter

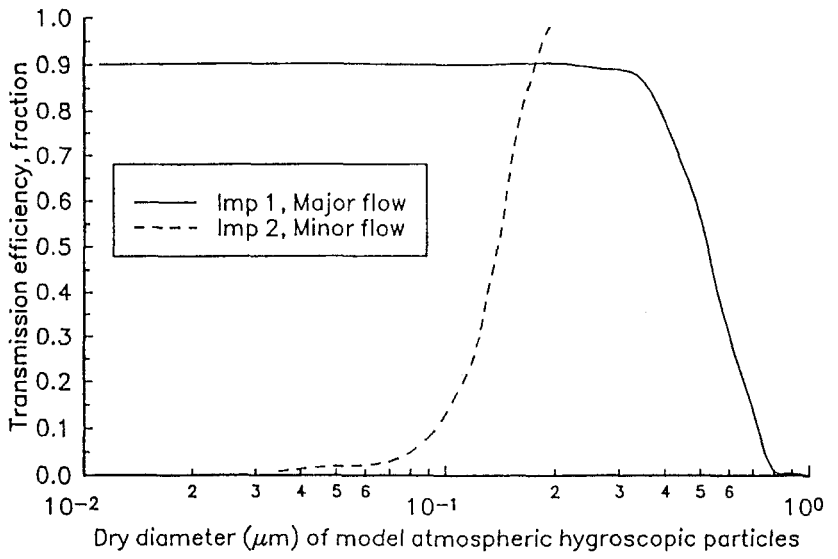

FIGURE 5. Measured efficiency curve for the major flow of impactor 1 (solid curve), and for the haze chamber impactor 2 minor flow combination (dashed curve).

2, except for the constant correction factor to account for the flow discarded just upstream of impactor 2 (see Fig. 3). This transmission efficiency has a peak at about 0.25 μm, and a spread from 0.1 to 0.7 μm. The expected mass distribution on filter 2 is the product of this efficiency and the mass distribution in the atmosphere, the latter having the shape shown in Fig. 2. The peak in Fig. 2 is also at about 0.25 μm, and thus one expects that the mass median diameter on filter 2 will be about 0.25 μm.

The solid curve of Fig. 6 shows the transmission efficiency for the major flow of impactor 2, and the dashed curve shows losses in impactor 2 as a fraction of the input concentration. The losses are not large enough to greatly reduce the loading on filter 2. The dotted curve shows measured transmission efficiencies from the inlet of the CFD to the minor flow of impactor 3. The CFD operated at a supersaturation of 1% while obtaining this curve, but for the air sampling program, the supersaturation was 0.6%, as discussed above. The slope of the dotted curve is mainly determined by the parabolic profiles of supersaturation and velocity in the CFD. This slope is expected to be unchanged for the lower operating supersaturation of the CFD, but the dotted curve would shift to the right.

The transmission efficiency from the inlet of the CFD to filter 3 is essentially the product of the solid curve and the dotted curve in Fig. 6. The transmission efficiency thus obtained has a peak at 0.1 μm, and a spread from about 0.05 to 0.2 μm. The shape of the mass distribution of the aerosol at the CFD is different from that in the atmosphere (Fig. 2), but it still has a peak larger than 0.1 μm, and thus the mass median diameter at filter 3 is expected to be larger than 0.1 μm.

MONTE CARLO MODEL OF SAMPLING SYSTEM PERFORMANCE

A Monte Carlo-type modeling method is used to compute the path of a particle through the sampling system. For each trajectory, the particle size is chosen at random from the assumed input particle size distribution. In addition, the particle com-

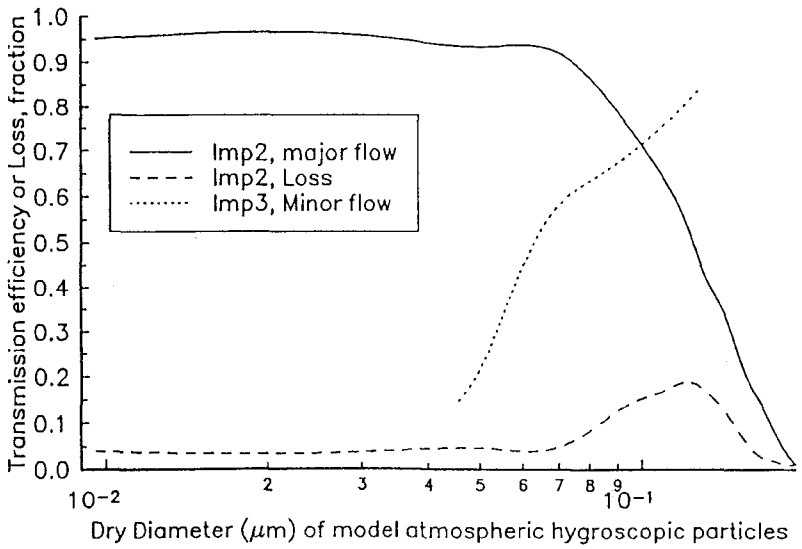

FIGURE 6. Measured efficiency curve for the haze chamber-impactor 2 major flow combination (solid curve), and for the CFD–impactor 3 minor flow combination, with the CFD operating at 1% supersaturation (dotted curve). The dashed curve is the loss fraction for the haze chamber–impactor 2 combination.

position is chosen at random to be either nonhygroscopic or hygroscopic. The measured transmission efficiency functions for each impactor as a function of Stokes number is an input to the model. The position of the particle between the plates inside the haze chamber and the CFD is randomly selected. The analytic solutions of Brown (1960) and Hatton and Turton (1962) are used to compute the temperature and vapor pressure fields in the haze chamber and in the CFD, respectively. Particle growth in these cloud chambers is calculated using the theory outlined by Carstens (1979) and Hagen (1979). The simulation is repeated for millions of particles in order to obtain a statistically significant result.

Monte Carlo simulations are presented for the case of an assumed Whitby, grand average, continental, particle size distribution (Whitby, 1978). Additionally, at any size, one particle in four is assumed to be the insoluble type described above, and the other three particles are assumed to be the hygroscopic type described above. The one-insoluble-particle-in-four assumption is not realistic. It would be more realistic to follow the trend of the data in Fig. 1. This one-in-four assumption is made so that the Monte Carlo method will give good counting statistics about the fate of the insoluble particles.

Figures 7 and 8 show the model prediction for the volume distributions at filters 2 and 3, respectively. The horizontal axis is dry particle diameter (D, μm) and the vertical axis is differential volume (μm^3 of particulate volume/cm^3 of atmospheric air drawn into the collection system) in the logarithmic differential size range. Consider Fig. 7, which is for filter 2. The top curve (squares) shows the input atmospheric volume distribution, the middle curve (circles) shows the hygroscopic particles deposited on filter 2, and the bottom curve (triangles) shows the concentration of insoluble particles. The mass median diameter of the particles at filter 2 is 0.27 μm.

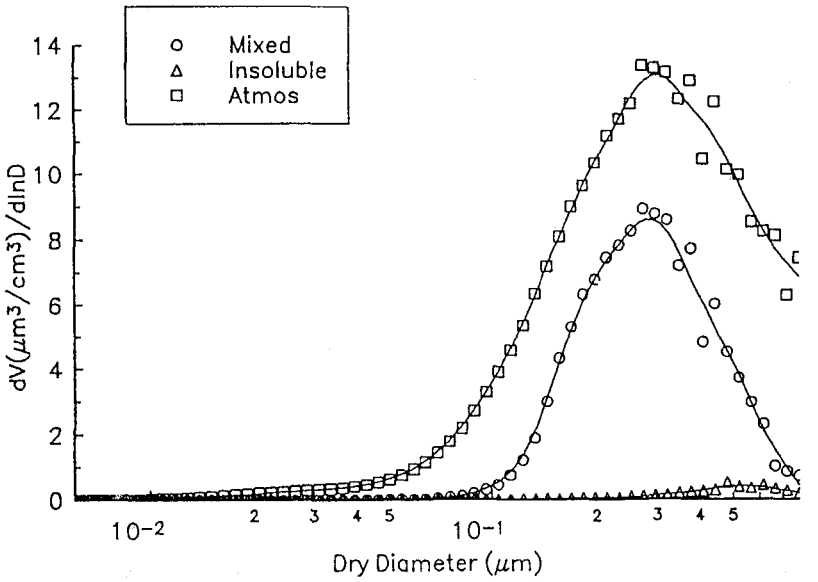

FIGURE 7. *Volume distributions of particles at filter 2 from simulation of the collection system. Top curve is the input atmospheric distribution. Middle curve is hygroscopic particles deposited on filter 2. Bottom curve is insoluble particles deposited on filter 2.*

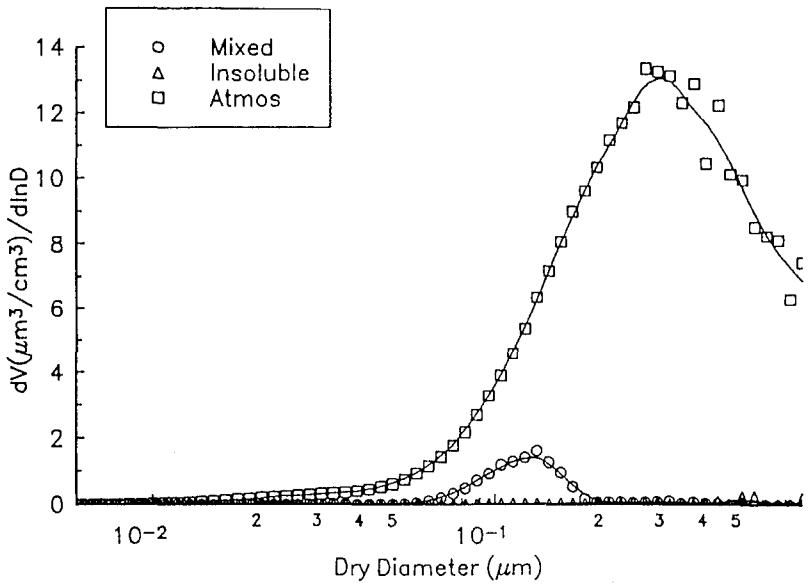

FIGURE 8. Volume distributions of particles at filter 3 from simulation of the collection system. Top curve is the input atmospheric distribution. Middle curve is hygroscopic particles deposited on filter 3. Bottom curve (lying nearly on the abscissa) is insoluble particles deposited on filter 3.

The rate of mass collection at filter 2 is calculated as follows. The area under the middle curve (10.2 $\mu m^3/cm^3$) is multiplied by the particle density (1.384 g/cm^3) and by the flow rate into the collection system (1948 m^3/day) to obtain a collection rate of 27.5 mg/day for the soluble particles. The same thing is done for the bottom curve to obtain a collection rate of (0.34 $\mu m^3/cm^3$) (1.000 g/cm^3) (1948 m^3/day) = 0.662 mg/day for the insoluble particles. Thus, the total collection rate at filter 2 is 28.2 mg/day.

Figure 8 is similar to Fig. 7, except that it shows particles deposited on filter 3. At filter 3, the mass median diameter is 0.12, and the loading due to the insoluble particles is 7% of the total loading. If the CFD is run at 1% operating supersaturation, the model indicates that the insoluble particle loading is about 20% of the total loading, due to insoluble particles 0.4 to 0.7 μm diameter. As discussed above, Fig. 1 indicates that there should be very few such insoluble particles, and the reason for reducing the CFD supersaturation is just in case measurements are made at a geographic location where there are relatively more insoluble particles than indicated by Fig. 1. The mass loading rate indicated by Fig. 8 for filter 3 is 3.13 mg/day.

Recall that filter 3M is the designation for the case where stage 8 of the MOUDI impactor is placed downstream of the minor flow of impactor 3 and upstream of filter 3M (Fig. 3). The volume distribution at filter 3M is obtained by multiplying the middle curve (circles) of Fig. 8 by the particle fraction not removed by the MOUDI. The fraction of particles not removed is assumed to be unity minus the fraction which are removed. The latter is obtained from the published (Marple et al., 1991) MOUDI stage 8 transmission curve, which has a cut-point of 0.056 μm diameter. The result indicates that the volume distribution at filter 3M peaks at 0.08 μm, and the mass median diameter is 0.075 μm. The total mass loading at filter 3M is about one order of magnitude lower than for filter 3.

RESULTS AND DISCUSSION

Filter 2 and 3 ambient air samples were collected at Rolla, MO, using the laboratory version of the sampling system, and at Champaign, IL and Big Bend National Park in southwestern Texas using the mobile version. Quartz fiber filter packs were used, so that for each filter location, there are two filters, a front filter and a back filter. The following front filter loading rates were observed, in units of mg/day, for sampling durations in the range 0.1–3 days. For filter 2, the rates are: Rolla, 3.77; Champaign, 4.25; and Big Bend, 2.27. For filter 3, the loading rates are: Rolla, 0.96; Champaign, 0.28; and Big Bend, 0.20. These mass loadings are not vastly different at the different geographic locations, but the chemical compositions are quite different. For example, there are nitrates in the Champaign sample, but not in the Rolla sample.

The model predictions of the filter loading rates depend on the ambient aerosol size distribution entered in the model, which does not necessarily reflect the actual sampling conditions. When put in the conventional form $N = CS^k$, where N is the number of droplets formed at supersaturation S, the CCN spectrum obtained from the model gives values for the fitted parameters of $C = 9750\ \text{cm}^{-3}$ and $k = 0.548$. In a long-term experimental study of the CCN spectra at Rolla, the corresponding values were found to be $C = 3990\ \text{cm}^{-3}$ and $k = 0.643$ (Alofs and Liu, 1981). If the values of k for the two spectra are considered about equal, then the filter loadings should be multiplied by a factor of 0.409 ($= 3990/9750$) in order to adjust the model results to the Rolla atmospheric aerosol. Using this normalization, the model prediction filter loading rates are 11.5, 1.28, and 0.13 mg/day at filters 2, 3, and 3M, respectively.

The observed Rolla loadings at filter 2 are 32.8% of those predicted by the Monte Carlo simulation, and the observed loadings at filter 3 are 75% of the value from the simulation. The most likely explanation of the discrepancies seems to be partial evaporation of particles, both within the cloud chambers and after they have been deposited on the filters. Nitrates are known to evaporate when collected on filters at reduced pressures (Zhang and McMurry, 1987), and the observed nitrate loading at filters 2 and 3 is very low for the Rolla samples. Other investigators have reported that semi-volatile organics sometimes produce a negative artifact, due to particulate evaporation, and sometimes produce a positive artifact, due to organic vapors being adsorbed onto the filters (Turpin et al., 1994). The positive organic artifact possibility was tested using a quartz denuder upstream of filter 2, with a denuder design like that described by Fitz (1990). The idea is that the denuder should reduce organic vapors going into the filter pack, thus reducing the part of the organic loading on the backup filter which is due to a positive artifact. The result for the present system is that the denuder did not reduce the loading on the backup filter. Thus, there is not much of a positive artifact, probably because the wet surfaces of the haze chamber serve as a sink for semi-volatile vapors. The denuder was also used upstream of filter 3, and again indicated that there was not much positive artifact, probably because the CFD itself acts as a denuder.

For the Rolla sampling, the mean loading at the backup filter 2 was 15% of the front filter 2 loading, and the loading at the backup filter 3 was 3.5% of the front filter 3 loading. The analysis of the backup filters at both filters 2 and 3 indicates that almost all of the loading is due to organics. Since the backup loading is not due to a positive artifact, it must be due to a negative artifact, i.e., due to particle evaporation from the front filter and subsequent adsorption of the resulting vapors onto the back filter. The negative artifact cannot be completely corrected for by adding the backup filter loading to that of the front filter because the backup filter does not absorb all of the vapor released from the front filter.

There is also evidence of particle evaporation within the haze chamber and the CFD. The dry size distribution at the minor flow of impactor 2 and at impactor 3 was measured with atmospheric air entering the

collection system. In these experiments, the sample airstream from the minor flow of either impactor 2 or 3 was mixed with dry filtered air in order to reduce the particulate to its dry size before measuring the particle size distribution. An optical particle counter was used to count those particles larger than 0.5 μm, and to cover the size range from 0.03 to 0.5 μm, the particles were passed through a DMA to select a "monodispersed" size. The size-classified aerosol was then passed into a TSI 3025A condensation nucleus counter to measure the number concentration. By determining the droplet counts over a range of EAC voltage settings and following the inversion technique of Hagen and Alofs (1983) to account for multiple charging, the particle size distribution was determined.

The results for the aerosol upstream of filters 2 and 3 are that the mass median diameters are 0.19 and 0.137 μm, respectively. Recall that the respective values from the Monte Carlo simulation are 0.27 and 0.12 μm. Thus, the measured size at filter 2 is smaller, but at filter 3 is slightly larger than the Monte Carlo model which does not account for particle evaporation.

CONCLUSION

Despite the small atmospheric concentrations of cloud condensation nuclei (CCN), milligram quantities of CCN material can be collected by scaling upward laboratory versions of a continuous flow diffusion cloud chamber and a haze chamber to accommodate an ambient flow of over 1 m^3/min. Such a sampling system is described, and tests showing its operating characteristics are reported. The system isolates three size classes of CCN, having mass median diameters of 0.27, 0.12, and 0.075 μm diameter, which are collected on filters 2, 3, and 3M, respectively. These sizes are obtained by a Monte Carlo simulation of the system, and do not account for any particle evaporation, whereas tests described above indicate that there is particle evaporation. The same simulation indicates that for the Missouri sampling site, the collection rates are 11.5, 1.28, and 0.13 mg/day at filters 2, 3, and 3M, respectively. The observed collection rates at Rolla are 32.8% and 75% of the rates predicted by the simulation at filters 2 and 3, respectively. The lower observed collection rates are ascribed to particle evaporation both within the cloud chambers and on the filters. Evidence indicates that the wet surfaces of the cloud chambers serve as a denuder which prevents a positive artifact for organics seen on the filters.

The mass concentrations at Rolla, MO and at Champaign, IL, as measured by two different versions of the apparatus, are similar. The mass concentrations at a remote site in Big Bend National Park in southwestern Texas are also similar.

This work was sponsored by the Department of Energy under Contract DE F02 90ER51017.

References

Alofs, D. J. (1978). Performance of a Duel Range Cloud Nucleus Counter, *J. Appl. Met.* 15:350–354.

Alofs, D. J., and Liu, T. H. (1981). Atmospheric Measurements of CCN in the Supersaturation Range 0.013–0.681%, *J. Atmos. Sci.* 38:2772–2778.

Alofs, D. J., and Trueblood, M. B. (1983). Solubility Measurements of Aerosols in the Greenfield Gap to Determine the Efficiency of In-Cloud Scavenging by Nucleation, in *Precipitation Scavenging, Dry Deposition, and Resuspension* (H. R. Pruppacher, R. G Semonin, and W. G. N. Slinn, eds.). Elsevier, Amsterdam, Vol. 1, pp. 483–491.

Alofs, D. J., Hagen, D. E., and Trueblood, M. B. (1989). Measured Spectra of the Hygroscopic Fraction of Atmospheric Aerosol Particles, *J. Appl. Met.* 28:126–136.

Brown, G. M. (1960). Heat and Mass Transfer in a Fluid in Laminar Flow in a Circular or Flat Conduit, *AIChE J.* 6:179–183.

Carrier, W. H., and Lindsay, D. C. (1924). The Temperature of Evaporation of Water into the Air, *Trans. ASME* 46:739–780.

Carstens, J. C. (1979). Droplet Growth in the Atmosphere by Condensation: Application to Cloud Physics, *Adv. Colloid Interface Sci.* 10:285–314.

Charlson, R. J., Lovelock, J. E., Andreae, M. O., and Warren, S. G. (1987). Oceanic Phytoplankton, Atmospheric Sulfur, Cloud Albedo and Climate, *Nature* 326:655–661.

Charlson, R. J., Schwartz, S. E., Hales, J. M., Cess, R. D., Coakley, Jr., J. A., Hansen, J. E., and Hofmann, D. J. (1992). Climate Forcing by Anthropogenic Aerosols, *Nature* 255:423–430.

Cken, B. T., and Yeh, H. C. (1987). An Improved Virtual Impactor: Design and Performance, *J. Aerosol Sci.* 18:203–214.

Ensor, D. E., Charlson, R. J., Ahlquist, N. C., Whitby, K. T., Husar, R. B., and Liu, B. Y. H. (1972). Multiwavelength Nephelometer Measurements in Los Angeles I. Comparison of Calculated and Measured Light Scattering, *J. Colloid Interface Sci.* 39:242–251.

Fitz, D. R. (1990). Reduction of the Positive Organic Artifact on Quartz Filters, *Aerosol Sci. Technol.* 12:142–148.

Fitzgerald, J. W., Hoppel, W. A., Vietti, M. A. (1982). The Size and Scattering Coefficient of Urban Aerosol Particles at Washington, DC as a Function of Relative Humidity, *J. Atmos. Sci.* 39:1838–1852.

Fitzgerald, J. W. (1991). Marine Aerosols: A Review, *Atmos. Environ.* 25A:533–545.

Hagen, D. E. (1979). A Numerical Cloud Model for the Support of Laboratory Experiment, *J. Appl. Met.* 18:1035–1043.

Hagen, D. E., and Alofs, D. J. (1983). Linear Inversion Method to Determine Aerosol Size Distributions from Measurements with a Differential Mobility Analyzer, *Aerosol Sci. Technol.* 2:465–475.

Hänel, G. (1976). The Properties of Atmospheric Aerosol Particles as Functions of the Relative Humidity at Thermodynamic Equilibrium with the Surrounding Moist Air, in *Advances in Geophysics* (H. E. Landsberg and J. Van Mieghem, eds.), Academic, New York, Vol. 19, pp. 73–188.

Havison, L. (1985). The Segregation of Aerosols by Cloud-Nucleating Activity, Part II: Design, Construction, and Testing of a High-flux Thermal Diffusion Cloud Chamber for Mass Separation, *J. Climate and Appl. Met.* 24:3302–3310.

Hatton, A. P., and Turton, J. S. (1962). Heat Transfer in the Thermal Intry Length with Laminar Flow Between Parallel Walls at Unequal Temperatures, *Int. J. Heat Transfer* 5:673–679.

Hering, S. V., Flagan, R. C., and Friedlander, S. K. (1978). Design and Evaluation of New Low-Pressure Impactor. I, *Environ. Sci. Technol.* 12:667–673.

Hileman, B. (1990). Biomass Burning: Environment Hurt More Than Thought, *Chem. Eng. News* 68:4–5.

Hudson, J. G. (1991). Observations of Anthropogenic Cloud Condensation Nuclei, *Atmos. Environ.* 25A:2449–2455.

Hudson, J. G., Hallett, J., and Rogers, C. F. (1991). Field and Laboratory Measurements of Cloud-forming Properties of Combustion Aerosols, *J. Geo. Res.* 96:10,847–10,829.

Kiehl, J. T., and Briegleb, B. P. (1993). The Relative Role of Sulfate Aerosols and Greenhouse Gases in Climate Forcing, *Science* 250:311–314.

Laktionov, A. G. (1972). A Constant Temperature Method of Determining the Concentrations of Cloud Condensation Nuclei, *Izv. Acad. Nauk. SSSR. Fiz. Atmos. Okeana.* 8:672–677.

Liu, B. Y. H., and Pui, D. Y. H. (1974). A Submicron Aerosol Standard and the Primary Absolute Calibration of the Condensation Nuclei Counter, *J. Colloid Interface Sci.* 47:155–171.

Marple., V. A., Rubow, K. L., and Behm, S. M. (1991). A Microorface Uniform Deposit Impactor (MOUDI): Description, Calibration, and Use, *Aerosol Sci. Technol.* 14:434–446.

Novakov, T., and Penner, J. E. (1993). High Contribution of Organic Aerosols to Cloud-Condensation-Nuclei Concentrations, *Nature* 365:823–826.

Pitchford, M. L., and McMurry, P. H. (1994). Relationship Between Measured Water Vapor Growth and Chemistry of Atmospheric Aerosol for Grand Canyon, Arizona, in Winter 1990, *Atmos. Environ.* 28:827–839.

Pruppacher, H. R., and Klett, J. D. (1978). *Microphysics of Clouds and Precipitation.* Reidel, Boston.

Schwartz, S. E. (1996). The Whitehouse Effect-Shortwave Radiative Forcing of Climate by Anthropogenic Aerosols: An Overview, *J. Aerosol. Sci.* 27:359–382.

Sparrow, E. M., and Chen, T. S. (1969). Mutually Dependent Heat and Mass Transfer in Laminar Duct Flow, *AIChE J.* 15:434–441.

Svenningsson, B., Hansson, H. C., Wiedensohler, A., Noone, K., Ogren, J., Hallberg, A., and Colvile, R. (1994). Hygroscopic Growth of Aerosol Particles and its Influence on Nucleation Scavenging in Cloud: Experimental Results from Kleiner Feldberg, *J. Atmos. Chem.* 19:129–152.

Turpin, B. J., Huntzicker, J. J., and Hering, S. V. (1994). Investigation of Organic Aerosol Sampling Artifacts in the Los Angeles Basin, *Atmos. Environ.* 28:3061–3071.

Twoney, S., and Wojcieshowski, T. A. (1967). Observations of the Geographical Variations of Cloud Nuclei, *J. Atmos. Sci.* 26:684–688.

Twoney, S. (1971). The Composition of Cloud Nuclei, *J. Atmos. Sci.* 28:377–381.

Twoney, S. A. Piepgrass, M., and Wolfe, T. L. (1984). An Assessment of the Impact of Pollution on Global Cloud Albedo, *Tellus* 36B:356–366.

Warner, J., and Twomey, S. (1967). The Production of Cloud Nuclei by Cane Fires and the Effect on Cloud Droplet Concentration, *J. Atmos. Sci.* 24:707–707.

Whitby, K. T. (1978). The Physical Characteristics of Sulfur Aerosols, *Atmos. Environ.* 12: 135–159.

Wigley, T. M. L. (1989). Possible Climate Change Due to the SO_2-derived Cloud Condensation Nuclei, *Nature* 339:365–367.

Zhang, X. Q., and McMurry, P. H. (1987). Theoretical Analysis of Evaporative Losses from Impactor and Filter Deposits, *Atmos. Environ.* 21:1779–1789.

Zhang, X. Q., McMurry, P. H., Hering, S. V., and Casuccio, G. S. (1993). Mixing Characteristics and Water Content of Submicron Aerosols Measured in Los Angeles and at the Grand Canyon, *Atmos. Environ.* 27A: 1593–1607.

Received April 14, 1995; revised July 8, 1996 and October 10, 1996.